

VERIFYING THE MASTER SINTERING CURVE ON AN INDUSTRIAL FURNACE

Deborah C. Blaine¹, Seong-Jin Park¹, Randall M. German¹,
Jerry LaSalle² and Hill Nandi³

¹Center for Innovative Sintered Products
The Pennsylvania State University
University Park, PA 16801

²Polymer Technologies, Inc.
Clifton, NJ 07011

³CompAS Control, Inc.
Indiana, PA 15701

ABSTRACT

The Master Sintering Curve is a simple means of predicting density evolution during sintering. This model relies on the work-of-sintering concept, a time-temperature integral, to predict the degree to which a compact has approached the theoretical density limit. The model is characterized through a series of constant heating rate dilatometry experiments. In this paper, we verify that although the model is based on laboratory scale measurements, it is applicable to manufactured parts sintered in an industrial furnace. The research includes incorporating the model in furnace monitoring software that shows real-time density evolution in the factory setting. As an example, we use gas-atomized 17-4PH stainless steel, injection-molded using a water-based binder into thick bars and sintered in a pusher furnace in hydrogen.

INTRODUCTION

The Master Sintering Curve (MSC), developed by Johnson [1], is a sintering densification model that links thermal processing history (time-temperature profile) to the concurrent evolution of density in a porous body formed from powder. It is based on diffusional sintering theory, represented in a combined-stage sintering equation [2]. Various studies on several powder material systems [1, 2] have shown that the MSC sinter model gives accurate predictions of density evolution, and can be used to determine the dominant sintering mechanisms through analysis of the diffusional activation energy.

In this study, a gas-atomized 17-4PH stainless steel powder is injection-molded and sintered to form a dense material. Analysis of the microstructural evolution of this powder during sintering [4] shows that below 1200°C the microstructure is a mixture of pores and austenite. However, above 1200°C a new δ -ferrite phase starts to form along grain boundaries and at pores. Through monitoring the sintering shrinkage [4], it is seen that there is a steep increase in the densification rate at 1200°C, indicating that the δ -ferrite phase offers a faster diffusion path, thus influencing the sintering kinetics of this material.

As the MSC model is defined by a single activation energy over the entire sintering regime, it fails to predict the influences of phase changes on sintering, as will be shown in this study. To overcome this obstacle, a modified version of the MSC is developed here for 17-4PH stainless steel. This two-phase

MSC splits the sintering regime into two regions about 1200°C. Constant heating rate dilatometry experiments are used to characterize both the original single phase MSC model, as well as the two-phase model. Through these laboratory scale experiments, accurate sintering models are developed for this system. These models are programmed into furnace monitoring and control software that are linked to an industrial pusher furnace, thus allowing for realtime monitoring of density evolution as the parts travel through the furnace.

To verify that the MSC models provide accurate prediction of sintered density in an industrial setting, a series of sintering experiments are performed in the pusher furnace. Analysis of the experimental results shows that the modified two-phase MSC model predicts sintered density accurately, within 2% of measured values.

EXPERIMENTAL WORK

The powder used in this study is a gas-atomized 17-4PH stainless steel (UFP). The powder characteristics are given in Table 1. The powder was compounded at 55vol.% solids loading using the Powderflo® water-based agar binder. Samples for the dilatometry experiments used to characterize the MSC models were cut from the gates of injection-molded samples. Samples of varying sizes were cut from thick injection molded bars for the verification experiments run in the pusher furnace. Table 2 gives the mean dimensions (rounded to the nearest 0.5mm, with standard deviations on each dimension less than 0.2mm) and green density of the five sizes cut for the verification experiments. Five samples were cut at each size. All of the green samples were dried in a convection oven at 60°C in air for 1h.

Table 1. Powder characteristics of the gas-atomized 17-4PH stainless steel powder

particle size	D ₁₀	D ₅₀	D ₉₀
laser diffraction, wet measurement	4.74µm	10.21µm	16.95µm
density	apparent	tap	pycnometer
	3.75g/cm ³	4.63g/cm ³	7.69g/cm ³

Table 2. Green dimensions for verification experiment samples

sample ID	dimensions, mm	density, g/cm³
LB	170.5 x 17.5 x 10	4.81 ± 0.02
A	36 x 17.5 x 13.5	4.78 ± 0.05
B	12.5 x 12 x 12	4.73 ± 0.02
C	31 x 17.5 x 10	4.72 ± 0.02
D	18 x 10 x 10.5	4.73 ± 0.04

The samples used for the dilatometer experiments were initially thermally debound in a retort furnace (Lindberg) under flowing hydrogen using the following thermal cycle: 2°C/min ramp with holds at 60°C for 1h, 110°C for 1h, and 600°C for 2h, followed by cooling in the furnace at 5°C/min. The thermal profiles for dilatometer experiments used to characterize the MSC are given in Table 3. The experiments were performed in flowing hydrogen (-40°C dewpoint, 0.5l/s flowrate) in a vertical pushrod dilatometer (Anter). The sintering shrinkage results are shown in Figure 1.

The experiments used to verify the MSC were run, under flowing hydrogen, in a continuous pusher furnace (CM Furnaces) that has 6 preheat zones and 3 high heat zones. Each zone is 670mm long, with a buffer zone of 335mm between the preheat and high heat zones. The pushrate in the furnace was 7.5mm/min. Five different cycles were used to produce a range of different sintering scenarios. The zone set temperatures are given in Table 4. One sample from each of the size groups in Table 2 was used for each cycle in Table 4. The sintered samples were measured and weighed, and the density was also

evaluated using the Archimedes water immersion method, except for the sample labeled LB which was too large to be immersed in which case the density was calculated using the dimensions and mass. The final sintered density and shrinkage is reported in Figure 2 as an average over all the different size samples for each cycle. The average shrinkage was the average over all three dimensions, length, width and height.

Table 3. Thermal profiles for MSC characterization dilatometer experiments

cycle	ramp 1	hold 1 (1h)	ramp 2	hold 2 (1h)
1	10°C/min	1010°C	7°C/min	1365°C
2	10°C/min	1010°C	5°C/min	1365°C
3	10°C/min	1010°C	1.67°C/min	1365°C
4	7°C/min	1200°C	-	-
5	5°C/min	1200°C	-	-

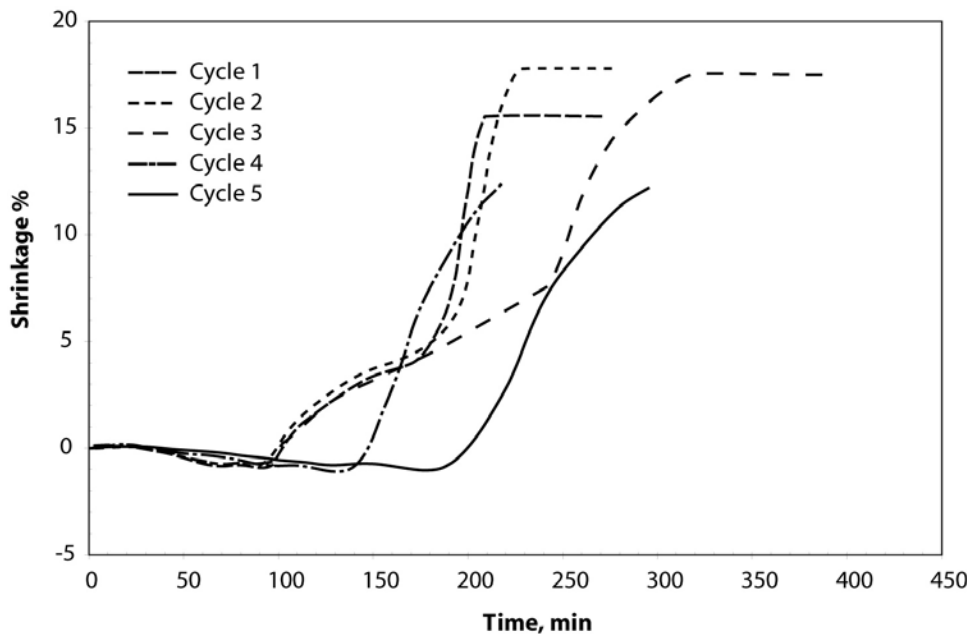


Figure 1. Sintering shrinkage results from dilatometer experiments used to characterize the MSC.

Table 4. Zone setpoint temperatures for pusher furnace verification experiments

cycle → zone ↓	A	B	C	D	E
preheat 1	90°C				
preheat 2	180°C				
preheat 3	350°C				
preheat 4	500°C				
preheat 5	650°C				
preheat 6	950°C				
high heat 1	1000°C	1000°C	1000°C	1000°C	1150°C
high heat 2	1100°C	1100°C	1200°C	1200°C	1300°C
high heat 3	1100°C	1200°C	1200°C	1300°C	1320°C

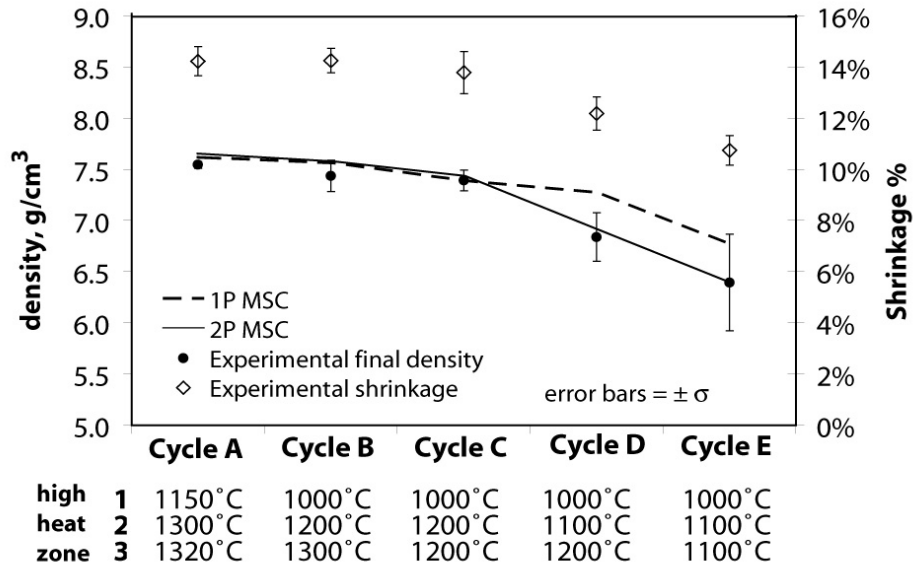


Figure 2. Sintered density and shrinkage results of MSC verification experiments run in the pusher furnace, with a comparison of the MSC predicted density.

MODEL DEVELOPMENT

The original MSC was developed by Johnson and Su [1] by relating the density evolution during sintering of a porous body to the thermal history through a time-temperature (t - T) integral, sometimes called the work-of-sintering, θ [4]

$$\theta = \int_b^t \frac{1}{T} \exp\left(-\frac{Q}{RT}\right) dt \quad (1)$$

where R is the universal gas constant, and Q is the apparent activation energy for sintering, a characteristic parameter of the MSC. Generally, the apparent activation energy is calculated by minimizing the mean square residual between constant heating rate dilatometer experiments and the MSC model [1,3]. If there is insufficient experimental data available to determine the apparent activation energy, published values for the grain boundary activation energy can be used [6].

It has been shown that a sigmoid function [6,7] provides a good fit between the relative density, ρ , reported relative to the powder pycnometer density, and the natural logarithm of the work-of-sintering, $\ln \theta$. The sigmoid equation used to define the MSC is

$$\rho = \rho_o + \frac{1 - \rho_o}{1 + \exp\left(-\frac{\ln \theta + a}{b}\right)} \quad (2)$$

where ρ_o is the initial relative density at the start of the sintering experiment, and a and b are constants. For this study, using the dilatometer experimental data, the initial relative density ρ_o was taken as the

green density at 0.55, the apparent activation energy was calculated as $Q = 350\text{kJ/mol}$, and the sigmoid function constants were found to be $a = 29.93$ and $b = 1.521$.

Using this single phase form of the MSC gives one smooth curve over the entire sintering regime, as shown in Figure 3. The change in shrinkage rate that occurs with the appearance of a δ -ferrite phase around 1200°C is not captured by this form of the sinter model. To overcome this problem, the sintering regime is divided into two regions about 1200°C , a low temperature and high temperature region.

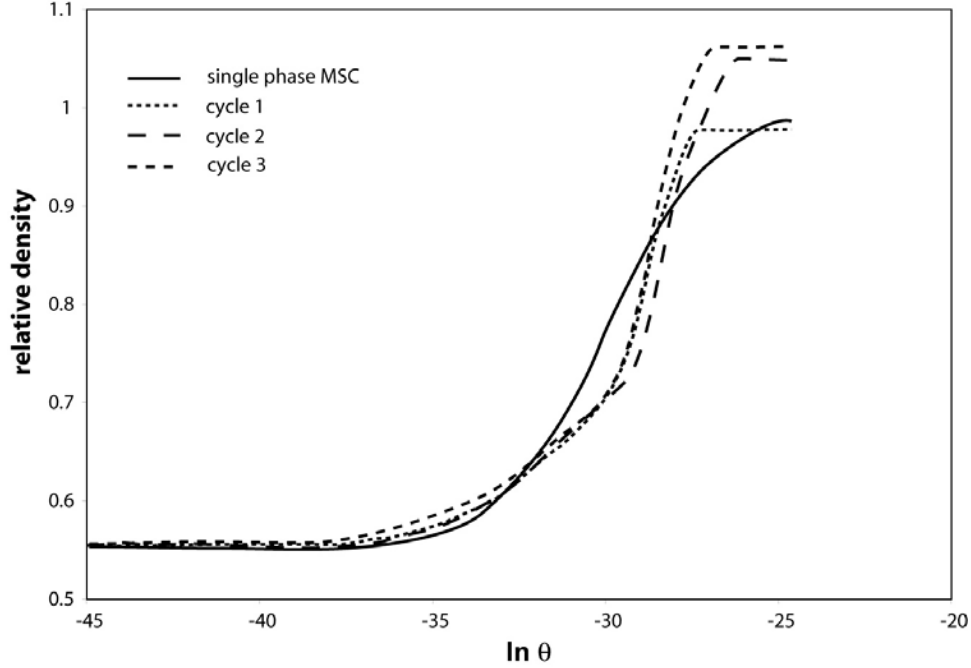


Figure 3. Single phase MSC compared against dilatometer experimental results.

The same form of the sigmoid equation in Equation 2 is used to fit the data in both regions, resulting in the following equations for each region:

low temperature region ($<1200^\circ\text{C}$)

$$\rho_1 = 0.55 + \frac{0.45}{1 + \exp\left(-\frac{\ln \theta_1 + 26.48}{2.006}\right)} \quad (3)$$

where θ_1 is calculated as in Equation 1 with $Q_1 = 321\text{kJ/mol}$.

high temperature region ($>1200^\circ\text{C}$):

$$\rho_2 = 0.55 + \frac{0.45}{1 + \exp\left(-\frac{\ln \theta_2 + \chi}{0.09512}\right)} \quad (4)$$

where the work-of-sintering θ_2 is calculated from 1200°C with $Q_2 = 350\text{kJ/mol}$, i.e.

$$\theta_2 = \theta_1(1200^\circ\text{C}, t_{1200^\circ\text{C}}) + \int_{1200^\circ\text{C}}^t \frac{1}{T} \exp\left(-\frac{Q_2}{RT}\right) dt \quad (5)$$

The χ parameter in the high temperature region defined by Equation 4 is not a unique point in θ as it is dependent on the thermal history (ramp and holds) of the low temperature region. It is determined by setting the low and high temperature equations equal to each other at 1200°C. For instance, for a 2°C/min ramp from 30°C to 1200°C, $\theta_1 = 4 \cdot 10^{-10}$ s/K, and setting Equation 3 and 4 equal to each other at this point gives a value for $\chi = 28.45$. Figure 4 shows the MSC plot for this hypothetical case.

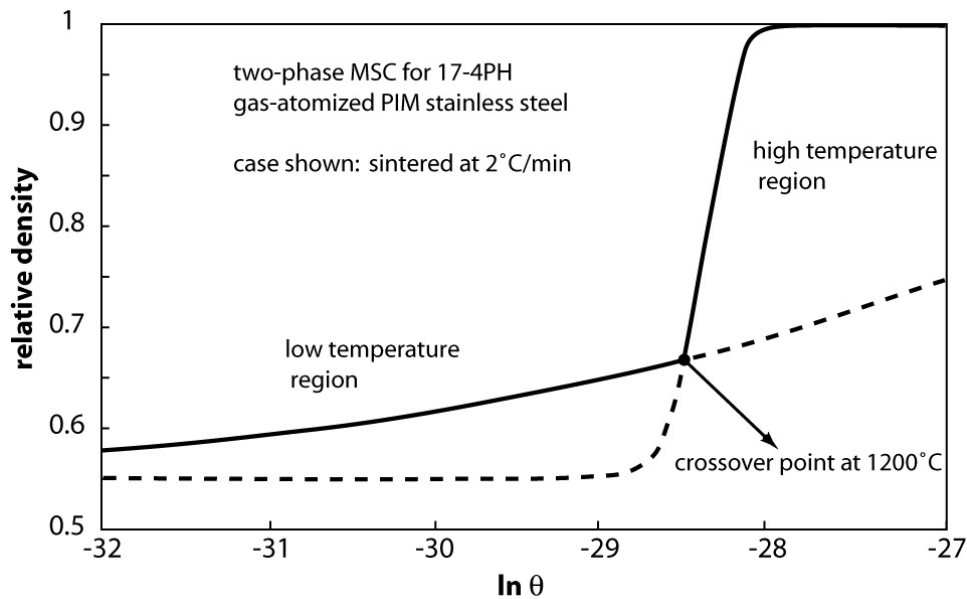


Figure 4. Two phase MSC showing crossover between low temperature, Equation 3, and high temperature, Equation 4, regions at 1200°C.

DISCUSSION

Applying both the single phase form of the MSC in Equation (2), and the two-phase form given in Equations (3), (4) and (5), to the verification experiments described allows the prediction of the sinter density for these experiments. The results are compared in Figure 2. The mean error between the experimentally measured and predicted sinter density is 2.82% for the single phase MSC, and 0.89% for the two-phase MSC. For cycles A, B, and C, both forms of the MSC predict the final density within one standard deviation, however, for the cycles that did not use high temperatures, cycles D and E, the single phase MSC did not offer a good prediction of the sinter density. As the verification experiments were performed in a continuous pusher furnace, it was not possible to have continuous shrinkage or density measurement throughout each cycle. The MSCs were verified by comparing the final density only.

Furnace control software LINEMOD[®] calculates the time and temperature profile in the furnace based on the thermal properties of the furnace and thermal load of the parts. The MSC equations given above can be included in the software to give a realtime log of the density evolution as the parts travel through the furnace. The design stage form of this software is called FURNXPRT[®], and an example of the density prediction screen, calculated using the MSC is shown in Figure 5.



Figure 5. Example of furnace design software FURNXPRT: density evolution module

CONCLUSIONS

The two phase MSC provides a more accurate model for sintering of gas-atomized 17-4PH stainless steel by fitting individual MSCs to the low temperature and high temperature regions. The crossover point between these two regions is marked at 1200°C by the appearance of a δ -ferrite phase along grain boundaries and at pores that contributes to an enhanced sintering rate in the porous body. For other materials that experience enhanced sintering rates due to second phases, such as liquid phase sintering or alloy additions, similar methods can be employed to yield accurate, yet simple sinter models over the entire sintering regime.

REFERENCES

- [1] Su, H. and Johnson, D. L., "Master Sintering Curve: A Practical Approach to Sintering", *J. Am. Ceram. Soc.*, Vol. 79, No. 12, 1996, pp. 3211-3217
- [2] Hansen, J. D., Rusin, R. P., Teng, M-H., and Johnson, D. L., "Combined-Stage Sintering Model", *J. Am. Ceram. Soc.*, Vol.75, No. 5, 1992, pp. 1129-1135
- [3] Johnson, D. L., "Finding and Utilizing the Master Sintering Curve", *Proceedings of Sintering 2003 (online)*, 2003, www.mri.psu.edu/conferences/sint03/#p1
- [4] Wu, Y., Blaine, D., Marx, B., Schlaefel, C., and German, R. M., "Sintering Densification and Microstructure Evolution of Injection Molding Grade 17-4PH Stainless Steel Powder", *Met. Mat. Trans. A*, Vol. 33A, July 2002, pp.2185-2194
- [5] Shoales, G.A., and German, R. M., "Combined Effects of Time and Temperature on Strength Evolution Using Integral Work-of-Sintering Concepts", *Met. Mat. Trans. A*, Vol. 30A, 1999, pp.465-470
- [6] Blaine, D. C., Gurosik, J. D., Park, S-J., Heaney, D., and German, R. M., "Master Sintering Curve Concepts as Applied to the Sintering of Molybdenum", *Met. Mat. Trans. A*, in press 2005
- [7] Teng, M-H., Lai, Y-C., and Chen, Y-T., "A Computer Program of Master Sintering Curve Model to Accurately Predict Sintering Results", *West. Pac. Earth Sc.*, Vol. 2, No. 2, 2002, pp.171-180